PAN POLSKA AKADEMIA NAUK

METROLOGY AND MEASUREMENT SYSTEMS

Index 330930, ISSN 0860-8229
www.metrology.pg.gda.pl

M&MS

GEOMAGNETIC DETECTION METHOD FOR PIPELINE DEFECTS BASED ON CEEMDAN AND WEP-TEO

Tao Zhang, Xinhua Wang, Yingchun Chen, Yi Shuai, Zia Ullah, Haiyang Ju, Yizhen Zhao

Beijing University of Technology, College of Mechanical Engineering and Applied Electronics Technology, 100 Ping Le Yuan, Chaoyang, Beijing 100124, China (*ztao891212@163.com*, ✉ *paper_bgdjd103@163.com*, +86 136 9326 4996, *ychen08089@163.com*, *shuaiyi_cjdx2008@126.com*, *engineerziaullah@yahoo.com*, *uhaiyang@emails.bjut.edu.cn*, *zhyizh@emails.bjut.edu.cn*)

Abstract

This paper presents a geomagnetic detection method for pipeline defects using *complete ensemble empirical mode decomposition with adaptive noise* (CEEMDAN) and *wavelet energy product* (WEP) – *Teager energy operator* (TEO), which improves detection accuracy and defect identification ability as encountering strong inference noise. The measured signal is first subtly decomposed via CEEMDAN into a series of *intrinsic mode functions* (IMFs), which are then distinguished by the Hurst exponent to reconstruct the filtered signal. Subsequently, the scale signals are obtained by using gradient calculation and discrete wavelet transform and are then fused by using WEP. Finally, TEO is implemented to enhance defect signal amplitude, completing geomagnetic detection of pipeline defects. The simulation results created by magnetic dipole in a noisy environment, indoor experiment results and field testing results certify that the proposed method outperforms *ensemble empirical mode decomposition* (EEMD)-gradient, EEMD-WEP-TEO, CEEMDAN-gradient in terms of detection deviation, *peak side-lobe ratio* (PSLR) and *integrated side-lobe ratio* (ISLR).

Keywords: geomagnetic detection, pipeline defects, magnetic field, filtering, data processing.

1. Introduction

Buried pipelines play a significant role in the national economic operation and human daily activities. Since oil & gas are flammable, explosive, and poisonous and can easy gather static electricity, accidents like fire, explosion and pollution could occur during the process of oil & gas storage and transportation. An explosion occurred in the pipeline often causes many casualties and huge economic losses, also resulting in serious pollution of the environment. Therefore, early damage inspection of the buried pipeline has become the top priority task.

In-line inspection (ILI) technologies, including *magnetic flux leakage* (MFL) [1], eddy current testing (ECT) [2], *ultrasonic technology* (UT) [3] and *electromagnetic acoustic transducers* (EMAT) [4], has been successfully employed to inspect pipeline defects. However, these technologies need pipeline pigs, constrained by space and angle, which always creates the congestion problem in the pipeline. In order to perform comprehensive inspection of a buried steel pipeline, non-contact testing technologies should be carried out without the need of excavation.

Article history: received on Aug. 13, 2018; accepted on Jan. 12, 2019; available online on Jun. 28, 2019, DOI: 10.24425/mms.2019.128363.

The *transient electromagnetic method* (TEM) [5] and Nopig technique [6] as representatives of external inspection technologies, has been widely applied to real detection. However, these methods require excitation sources which largely decrease their efficiency. The geomagnetic detection is a new technology that uses the magnetic field change created by geomagnetic field traverse pipeline defects to perform non-destructive testing [7, 8]. It measures the magnetic field with high-precision magnetic sensors to identify a possible defect existing in the buried steel pipeline. During the geomagnetic detection, the measured signal contains a great deal of noise caused by environmental disturbance, instrument zero/temperature drift and the detection platform instability, which adds to the real defect signal. Therefore, it is necessary to propose a method to filter noise from the measured signal. Nowadays, there are many filtering methods available. The wavelet transform decomposes a signal into low and high-frequency coefficients, which are screened by hard or soft threshold functions to filter noise [9]. However, the wavelet de-noising needs to predefine the basis function. The *empirical mode decomposition* (EMD) proposed by Huang [10], which could perform an adaptive decomposition of non-stationary and non-linear signals. The complex signals are expressed as the sum of multiple oscillatory functions, called multiple *intrinsic mode functions* (IMFs). The IMFs have a meaningful instantaneous frequency and carry the detailed information of the signal. The EMD has excellent filtering performance for noisy signals [11, 12]. However, the EMD is always hindered by mode mixing and false modes [13]. To overcome these shortcomings, the *ensemble empirical mode decomposition* (EEMD) was proposed by Wu [14], which effectively settled the EMD problem by adding a certain amount of Gaussian white noise. Based on the above advantages, some filtering methods based on EEMD are studied [15, 16]. However, the process of repeatedly adding noise often leads to residual noise and produces different numbers of modes by different iterations, which reduces the filtering performance. Therefore, Yeh developed the *complete ensemble empirical mode decomposition with adaptive noise* (CEEMDAN) [17], which achieved insignificant reconstruction errors and high precision decomposition by adding the adaptive Gaussian white noise to each stage of EMD. At present, this technology is applied to gear fault diagnosis [18], power load forecasting [19] and ECG signal de-noising [20]. However, the research on applying the CEEMDAN filtering to the magnetic signal is almost non-existing.

To study the defect identification method as signal filtering only is far not enough to pipeline detection. Li [21] studied the relationship between the detection distance and the defect signal by measuring the normal and tangential components of the magnetic field. The spectral analysis [22, 23] is a common technique employed in the fields of measurements and sensing systems. Because the frequency of magnetic field caused by buried pipeline defects is very low, this method is not suitable for the geomagnetic detection. Some scholars have researched defect identification methods. Song [24] used the wavelet transform to decompose and reconstruct the magnetic field, further recognizing the indoor pipeline defects. The gradient can provide a more clear interpretation of the defect region. Dubov [25] used the gradient peak of three-axis magnetic field intensity to locate defects in a buried oil & gas pipeline and an insulated process pipeline. However, a powerful method is still lacking as the working conditions of buried pipelines are too complex.

In this paper, we propose a method based on CEEMDAN and *wavelet energy product* (WEP) – *Teager energy operator* (TEO) to improve efficiency of the geomagnetic detection. The measured signal is first decomposed by CEEMDAN into a series of IMFs and a residue, and then valid modes are selected by the Hurst exponent to refactor the filtered signal. Subsequently, the gradient calculation and *discrete wavelet transform* (DWT) are used to obtain scale signals, which are then fused by WEP- TEO to detect pipeline defects.

2. Complete ensemble empirical mode decomposition with adaptive noise de-noising

2.1. Complete ensemble empirical mode decomposition with adaptive noise

CEEMDAN can alleviate the mode mixing problem in EMD and residual noise & additional modes in EEMD. The CEEMDAN process can be defined as follows:

1. Decompose $x + \alpha_0 n^{(j)}$ $(j = 1, \ldots, N)$ to obtain first IMF by EMD:

$$h_1 = \frac{1}{N} \sum_{j=1}^{N} h_1^{(j)}, \tag{1}$$

   where α_0 is the amplitude of the added white noise and $n^{(j)}$ is white noise occurring in the j-th ensemble trial. N is the total number of ensemble trials.
2. Calculate the first residue:

$$r_1 = x - h_1 . \tag{2}$$

3. Decompose $r_1 + \alpha_1 E_1(n^{(j)})$ to acquire the first mode and compute the second IMF:

$$h_2 = \frac{1}{N} \sum_{j=1}^{N} E_1 \left(r_1 + \alpha_1 E_1 \left(n^{(j)} \right) \right). \tag{3}$$

4. For $i = 2, \ldots, I$, compute the ith residue:

$$r_i = r_{i-1} - h_i . \tag{4}$$

5. Decompose $r_i + \alpha_i E_i(n^{(j)})$ to acquire the first mode and calculate the $(i+1)$-th IMF as:

$$h_{i+1} = \frac{1}{N} \sum_{j=1}^{N} E_1 \left(r_i + \alpha_i E_i \left(n^{(j)} \right) \right), \tag{5}$$

   where E_i represents the ith IMF obtained by EMD.
6. Repeat steps (4) to (5) until the residue cannot be longer decomposed. A signal x can be represented as:

$$x = \sum_{i=1}^{I} h_i + r_I . \tag{6}$$

2.2. IMFs selection method based on Hurst exponent

The Hurst exponent is an effective index to examine randomness of time series, which is used to distinguish signal IMFs and noise IMFs in this study. The calculation steps of Hurst exponent can be defined as follows:

1. For a time series x_i, $i = 1, 2, 3, \ldots, N$, set the window size $\tau = 1$.
2. Compute the standard deviation of x_i and record the point $(\tau, \tau \cdot \sigma_\tau)$.
3. Average data of adjacent points and overwrite the original data:

$$x_i = \frac{x_{2i-1} + x_{2i}}{2} . \tag{7}$$

4. Rescale appropriately as $N \leftarrow N/2$, $\tau \leftarrow 2\tau$.
5. When $N > 4$, repeat steps (2) to (4).
6. Plot a log-log graph and calculate its slope as the Hurst exponent h.

In this paper, we define IMFs of $h > 0.5$ as signal IMFs decomposed by CEEMDAN.

2.3. Application

The noisy signal is filtered to determine effectiveness of the CEEMDAN de-noising. A signal $x(t)$ comprises three periodic signals of differing frequencies:

$$x(t) = \cos(2\pi f_1 t) + \sin(2\pi f_2 t) + 2 * \sin(2\pi f_3 t), \tag{8}$$

where $f_1 = 3$, $f_2 = 5$, $f_3 = 11$, the length of data is 1024. A white Gaussian noise is added to the signal with the input *signal-to-noise ratio* ($\mathrm{SNR_{in}}$) of 0 dB. As shown in Fig. 1, the noisy signal is decomposed into 8 IMFs and a residue using CEEMDAN (the amplitude of the added white noise is 0.1 and the total number of ensemble trials is 300). It is difficult to identify which IMFs belong to the signal IMFs by direct observation. Subsequently, the Hurst exponent of each IMF is calculated; the results are shown in Table 1. According to the selection rule, IMF5-IMF8 are the signal IMFs, whereas IMF1-IMF4 are the noise IMFs. The filtered signal is reconstructed by summing all signal IMFs and the residue. The noisy signal is presented in Fig. 2a, and the original signal $x(t)$ and the filtered signal are shown in Fig, 2b. It can be seen that the filtered signal removes the redundant noise and recovers the actual signal waveform accurately.

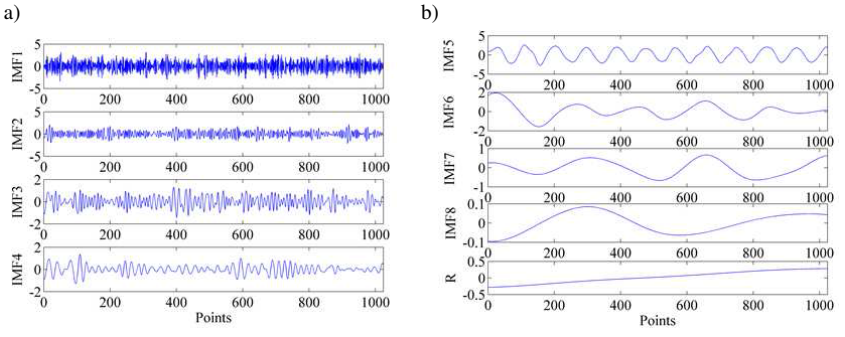

Fig. 1. The decomposition results using CEEMDAN. a) IMF1-IMF4; b) IMF5-IMF8 and residue.

Table 1. Hurst exponents of IMFs.

IMFs	IMF1	IMF2	IMF3	IMF4	IMF5	IMF6	IMF7	IMF8
Hurst exponent	0.2623	0.2175	0.1354	0.3003	0.7209	0.9234	0.9665	1

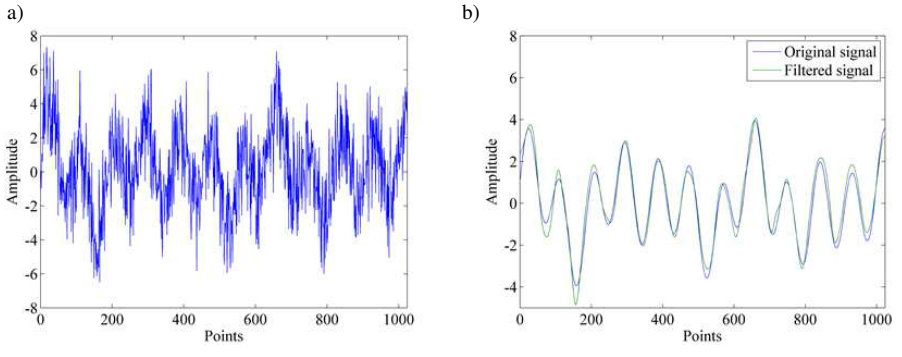

Fig. 2. The noisy and filtered signals. a) The noisy signal; b) the original and filtered signals.

3. Wavelet energy product – Teager energy operator method

3.1. Wavelet energy product

The wavelet transform has a good time-frequency characteristic and the ability to represent local features in the time and frequency domains. Let $\psi(t) \in L^2(R)$ and its Fourier transform satisfies the following conditions:

$$C_\psi = \int_{R^*} \frac{|\psi(\omega)|^2}{|\omega|} d\omega < \infty, \tag{9}$$

where R^* represents real numbers except for zero. $\psi(t)$ is called the mother wavelet. For signal $f(t)$, the continuous wavelet transform is defined as:

$$W_f(a,b) = \langle f(t), \psi_{a,b}(t) \rangle = \frac{1}{\sqrt{|a|}} \int_R f(t) \overline{\psi\left(\frac{t-b}{a}\right)} dt, \tag{10}$$

where a represents the scale parameter, b represents the translation parameter, and $\psi_{a,b}(t)$ represents the wavelet basis function.

For the real signal, a and b are discrete, and the DWT of signal $f(t)$ is denoted $W_f(j,k)$:

$$W_f(j,k) = \left\langle f(t), \psi_{j,k}(t) \right\rangle = \frac{1}{\sqrt{|a|}} \int_R f(t) \overline{\psi\left(\frac{t-b}{a}\right)} dt, \tag{11}$$

where $a = a_0^j$, $b = k a_0^j b_0$, $a_0 > 1$, $b_0 > 0$, $j \in Z$, and $k \in Z$.

According to the Mallat algorithm, the DWT decomposes a discrete signal $f(t)$ into two parts: the approximation and detail scales, which can be expressed as:

$$A_j = \sum_{k=-\infty}^{\infty} c_{j,k} \varphi_{j,k}(t), \tag{12}$$

$$D_j = \sum_{k=-\infty}^{\infty} d_{j,k} \psi_{j,k}(t), \tag{13}$$

where $\varphi_{j,k}(t)$ represents the scaling function, $\psi_{j,k}(t)$ represents the wavelet function, $c_{j,k}$ represents the scaling coefficient, and $d_{j,k}$ represents the wavelet coefficient.

According to the wavelet decomposition characteristics of noise and signal, the wavelet transforms of noise with different scales have no significant correlation, but the wavelet transforms of the signal with different scales are strongly correlated and the maximum value of correlation appears in the same location. Based on the above property, the *wavelet energy product* (*WEP*) is proposed to enlarge the defect signal amplitude and decrease the noise amplitude:

$$WEP_{i,j} = S_i \times S_j, \tag{14}$$

where S_i and S_j represent the scale signals of levels i and j, respectively.

3.2. Teager energy operator

The *Teager energy operator* (TEO) can enhance the feature of the transient signal, which is used to improve the defect identification ability. For an original signal x with amplitude A and frequency f, it can be expressed as a discrete form when the sampling frequency is f_s:

$$x_n = A\cos(\Omega n + \phi), \tag{15}$$

where $\Omega = 2\pi f/f_s$, ϕ is the initial phase angle. A, Ω and ϕ are obtained by solving the following equations:

$$\begin{cases} x(n) = A\cos(\Omega n + \phi) \\ x(n-1) = A\cos(\Omega(n-1) + \phi) \\ x(n+1) = A\cos(\Omega(n+1) + phi) \end{cases}. \tag{16}$$

Solving (16) gives:

$$A^2\sin^2(\Omega) = x_n^2 - x_{n+1}x_{n-1}\,. \tag{17}$$

When Ω is small enough, $\sin(\Omega) \approx \Omega$. When the sampling frequency is high enough, (17) can be rewritten as:

$$A^2\Omega^2 \approx x_n^2 - x_{n+1}x_{n-1}\,. \tag{18}$$

Therefore, TEO can be defined as:

$$J(x_n) = A^2\sin^2(\Omega) \approx A^2\Omega^2. \tag{19}$$

4. Geomagnetic detection for pipeline defect using CEEMDAN and WEP-TEO

In order to improve efficiency of the geomagnetic detection, a detection method based on CEEMDAN and WEP-TEO is proposed, a flowchart of which is shown in Fig. 3.

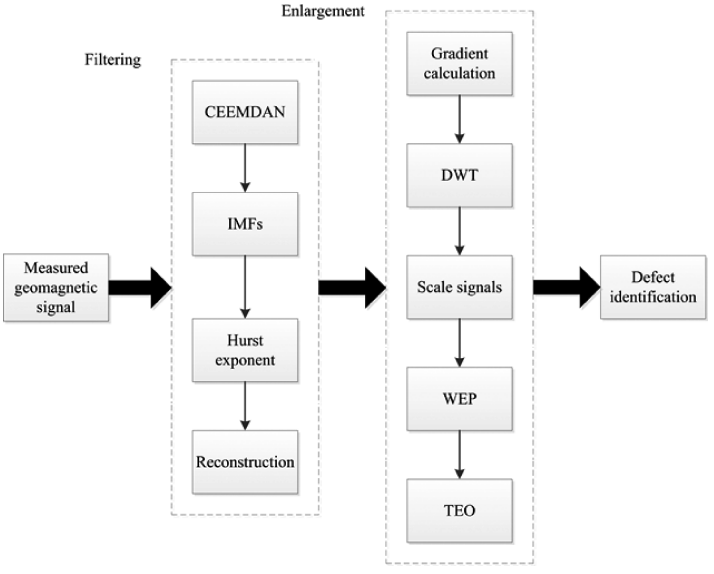

Fig. 3. A flowchart of CEEMDAN-WEP-TEO.

1. Decompose the measured signal by CEEMDAN into a series of IMFs and a residue.
2. Distinguish all IMFs by the Hurst exponent as signal IMFs and noise IMFs, and sum the signal IMFs and the residue to reconstruct the filtered signal.
3. Calculate the gradient of the signal, and then use DWT to obtain detail and approximation coefficients to construct the scale signals.
4. Adopt WEP to fuse different scale signals, and use TEO to enlarge the amplitude of the defect signal.
5. Identify the pipeline defect by seeking the peak of the final signal.

5. Simulation

Generally, a pipeline defect can be considered as a magnetic dipole as the distance between the defect and the measurement point is 2.5 times greater than the maximum dimension of the defect. If the magnetic moment is $\boldsymbol{m} = m_x\boldsymbol{i} + m_y\boldsymbol{j} + m_z\boldsymbol{k}$ and the displacement vector from the source to the measurement point is $\boldsymbol{r} = r_x\boldsymbol{i} + r_y\boldsymbol{j} + r_z\boldsymbol{k}$, the magnetic field vector is:

$$\boldsymbol{B} = \frac{\mu_0}{4\pi}\left[\frac{3(\boldsymbol{m}\cdot\boldsymbol{r})\boldsymbol{r}}{r^5} - \frac{\boldsymbol{m}}{r^3}\right], \tag{20}$$

where μ_0 is the permeability of vacuum. The magnetic moment $\boldsymbol{m}$ can be defined as:

$$\boldsymbol{m} = V\chi_m\boldsymbol{H}, \tag{21}$$

where V is the defect volume, χ_m is the magnetic susceptibility and $\boldsymbol{H}$ is the geomagnetic field intensity.

The defect signal is generated by the stress and the geomagnetic field, and its magnetic signal is obtained in the process of magnetomechanical coupling. The magnetic susceptibility can be expressed as:

$$\chi_m = \frac{2\mu_0 M_s^2}{9\lambda_s\sigma}, \tag{22}$$

where M_s is the saturation magnetization, λ_s is the magnetostriction coefficient and σ is the stress.

Assuming that the pipeline is subjected only to the internal pressure, both the hoop stress σ_h and the axial stress σ_a can be considered as invariable for the pipeline:

$$\sigma_h = PD/2\delta, \tag{23}$$

$$\sigma_a = PD/4\delta, \tag{24}$$

where P is the internal pressure, D is the diameter of the pipeline, δ is the thickness of the pipeline.

Figure 4 illustrates a defect on the pipeline upper surface located at the origin of coordinates, with a length $a = 0.1$ m, a width $b = 0.15$ m, a depth $c = 0.001$ m. $\lambda_s = 57$ ppm, $M_s = 1.76 \times 10^6$ A/m, $P = 3$ MPa, $D = 300$ mm, and $\delta = 10$ mm. The measurement length is $2L = 10$ m and the sampling interval is $s = 0.01$ m. The distance from the sensor to ground is $h_1 = 0.5$ m, the distance from ground to the pipeline upper surface is $h_2 = 1$ m. The geomagnetic field intensity is $H = 43.56$ A/m, the magnetic declination is $D = -6°$, the magnetic inclination is $I = 59°$.

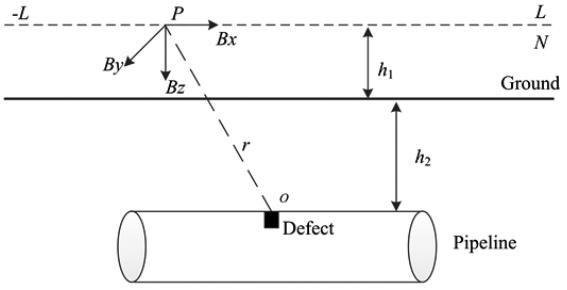

Fig. 4. A pipeline defect model.

The axial component of the defect magnetic signal generated by the model presented in Fig. 4 is considered as the input signal to evaluate the proposed method feasibility. First, we observe the filtering performance of EEMD de-noising and CEEMDAN de-noising. For EEMD and CEEMDAN, the amplitude of the added white noise is 0.1 and the total number of ensemble trials is 300. To ensure quantitative comparison, the output *signal-to-noise ratio* (SNR_{out}) and *root mean square error* (*RMSE*) are used to evaluate the filtering performance:

$$SNR_{\text{out}} = 10\log\left\{\frac{\sum_{i=1}^{n} s^2(i)}{\sum_{i=1}^{n}[s(i)-\hat{s}(i)]^2}\right\}, \tag{25}$$

$$RMSE = \sqrt{\frac{1}{n}\sum_{i=1}^{n}[s(i)-\hat{s}(i)]^2}, \tag{26}$$

where $s(i)$ is the original signal, $\hat{s}(i)$ is the de-noised signal, n is the number of sampling points.

Figure 5 presents the noisy signal $SNR_{\text{in}} = 5$ dB) and filtered signal using EEMD de-noising and CEEMDAN de-noising. It can be seen that both de-noising methods have the capability to filter out noise. Furthermore, the SNR_{out} and *RMSE* of two filtered signals are shown in Table 2. From Table 2 it can be seen that the SNR_{out} of CEEMDAN de-noised signal is higher than

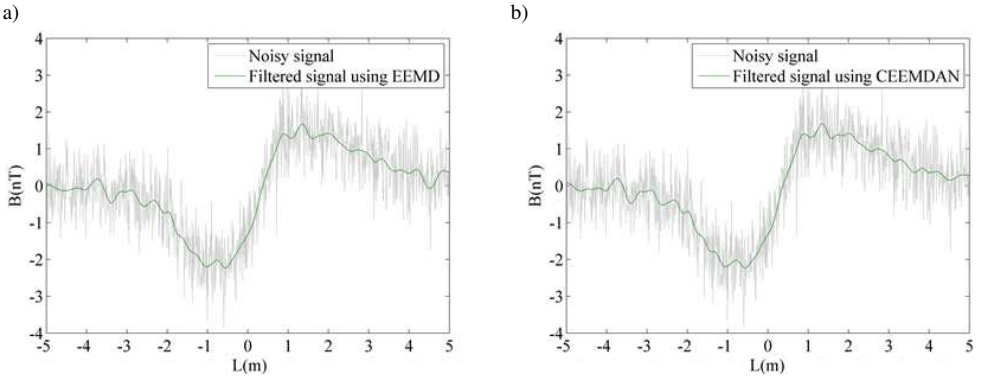

Fig. 5. The noisy signal and filtered signals: a) EEMD de-noising; b) CEEMDAN de-noising.

that of EEMD de-noised signal, and the *RMSE* of CEEMDAN de-noised signal is smaller than that of EEMD de-noised signal. In conclusion, the CEEMDAN de-noising has a better filtering performance than the EEMD de-noising.

Table 2. SNR_{out} and *RMSE* values of two filtered signals.

Indexes	EEMD denoising	CEEMDAN denoising
SNR_{out}	18.1247	18.9664
RMSE	0.1347	0.1222

We use EEMD-gradient, EEMD-WEP-TEO, CEEMDAN-gradient, and the proposed method to process the magnetic signal in the noisy environment. The wavelet basis function is sym8, the number of decomposition layers is 6, and the last three scale signals are selected to be fused. The detection deviation, *peak side-lobe ratio* (PSLR) and *integrated side-lobe ratio* (ISLR) are used to evaluate accuracy and distinguishability. The detection deviation is defined as the absolute value of the difference between the signal peak location L_p and the actual defect location L_a:

$$D = \left| L_p - L_a \right| . \tag{27}$$

PSLR [26] and ISLR [27] are indicators used in the radar signal; they are determined as:

$$\text{PSLR} = 10 \log \frac{p_s}{p_m} , \tag{28}$$

$$\text{ISLR} = 10 \log \frac{E_s}{E_m} , \tag{29}$$

where p_s is the value of the highest side-lobe (the second highest peak), p_m is the value of the main-lobe (the highest peak), E_s represents all side-lobe energy and E_m stands for main-lobe energy. Smaller PSLR and ISLR values mean better detection capability.

Figure 6 presents the detection results of four methods. It can be seen that the detection results based on EEMD-gradient and CEEMDAN-gradient have a poor effect. Further, the detection deviation, PSLR, and ISLR based on four detection results are presented in Table 3. The deviation of detection result based on the proposed method is smaller than those of other methods. In addition, the PSLR of detection result based on the proposed method is higher than that of EEMD-gradient by approximately 3.4 dB, EEMD-WEP-TEO by approximately 3.2 dB, CEEMDAN-gradient by approximately 2.5 dB. For the ISLR index, the ISLR of detection result based on the proposed method is higher than that of EEMD-gradient by approximately 6.4 dB, EEMD-WEP-TEO by approximately 1.1 dB, CEEMDAN-gradient by approximately 5.5 dB. As expected, the proposed method has better detection accuracy and defect identification ability than other conventional detection methods. Therefore, the proposed method is more suitable as a detection method for recognizing pipeline defects.

Table 3. The evaluation indexes of different simulation results.

Indexes	EEMD-gradient	EEMD-WEP-TEO	CEEMDAN-gradient	Proposed method
Detection deviation(m)	0.27	0.2	0.25	0.02
PSLR (dB)	−0.4139	−0.6695	−1.3128	−3.8494
ISLR (dB)	8.5171	3.2121	7.6752	2.1322

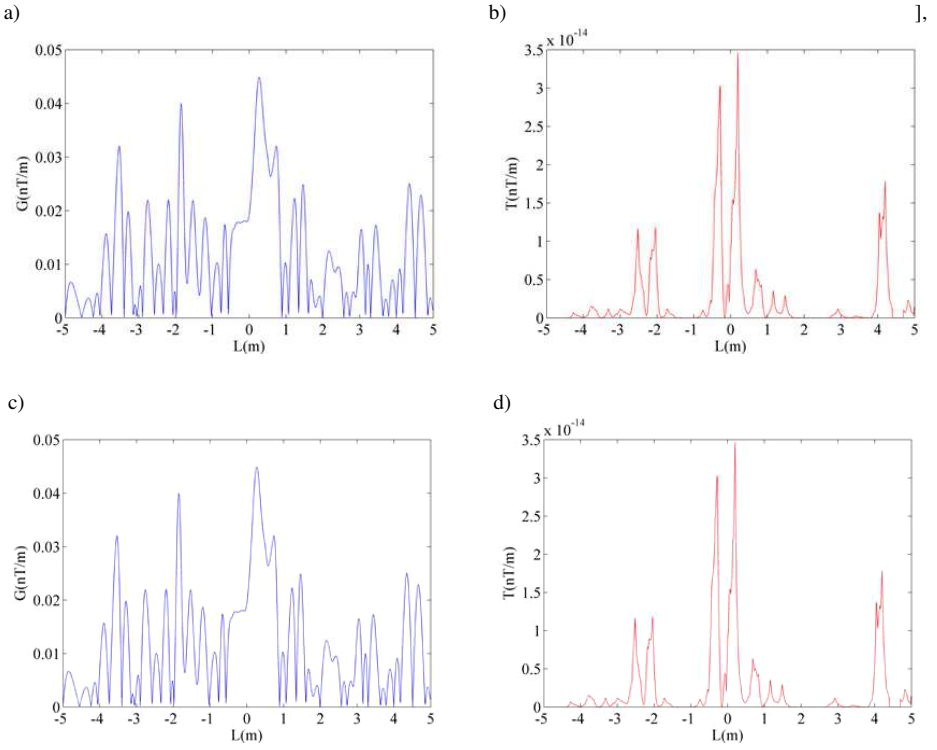

Fig. 6. The simulation results of different methods: a) EEMD-gradient; b) EEMD-WEP-TEO; c) CEEMDAN-gradient; d) the proposed method.

6. Experimental verification

6.1. Indoor experiment

The indoor experiment was performed to understand the effect of the proposed method. Fig. 7a shows the experimental system, which consists of a magnetic sensor, a high-speed acquisition card, a three-dimensional console and a computer. The magnetic sensor is a Mag-03 three-axis

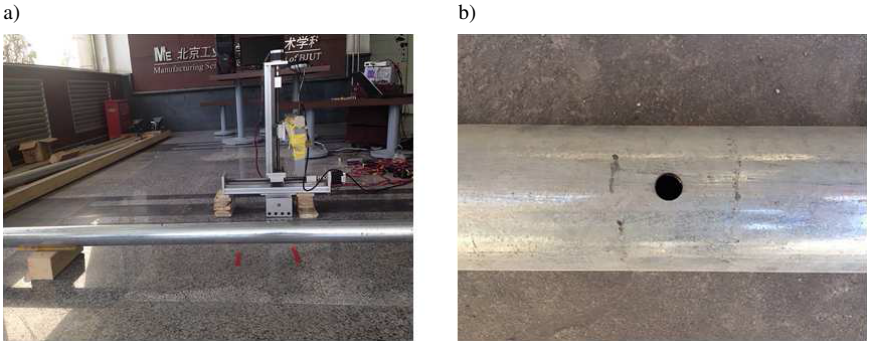

Fig. 7. The indoor experiment of geomagnetic detection: a) the experimental system; b) the hole defect.

fluxgate magnetometer (noise < 10 pTrms/$\sqrt{\text{Hz}}$ at 1 Hz and the measurement range is ±1000 μT). The acquisition card is an NI USB6281 (the resolution is 18 bits and the sampling rate is 625 kS/s). The test pipeline is made of Q235 steel with a diameter of 75 mm and a wall thickness of 3 mm. The lift-off is three times the pipe diameter and the detection length is 180 mm. Fig. 7b shows the 12 mm diameter hole made on the outer surface of the pipeline, located at 90 mm along the detection route.

The axial component of the measured magnetic field signal and the gradient signal are shown in Fig. 8. Due to the noise influence, the gradient signal has lost its ability to identify defects. First, EEMD de-noising and CEEMDAN de-noising were used to filter out noise in the measured signal. Since the original signal was unknown, the SNR_{out} and RMSE could not be calculated. The *detrended fluctuation analysis* (DFA) is an analysis method based on the stochastic process theory and chaotic dynamics, used to detect the physical characteristics of time series. The scaling exponent represents the roughness of time series: its larger value means a smoother time series. DFA has been successfully used to evaluate the filtering performance for the impact signal [28] and the pipeline leakage signal [29]. The scaling exponents of two de-noised signals are equal to 1.9498 and 1.9676, respectively, which shows that CEEMDAN de-noising has a better filtering performance than EEMD de-noising.

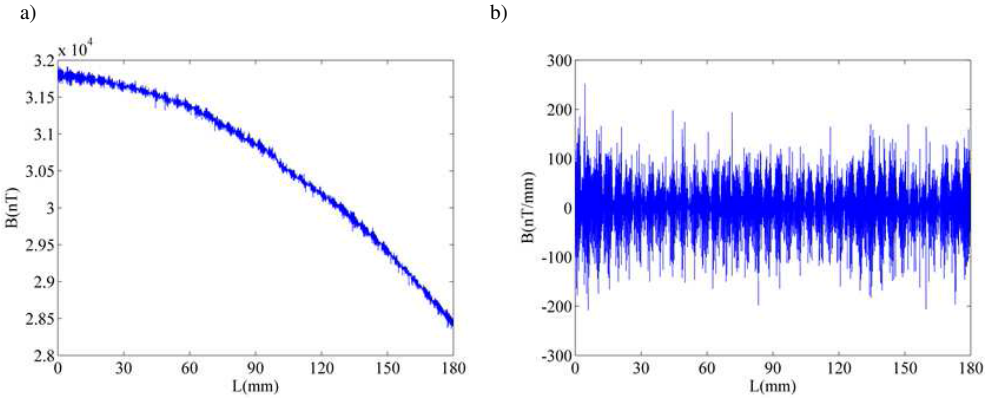

Fig. 8. The measured signal in the indoor experiment: a) the original signal; b) the gradient signal.

Figure 9 presents the detection results based on EEMD-gradient, EEMD-WEP-TEO, CEEMDAN-gradient and the proposed method. The detection deviation, PSLR, and ISLR of four detection results are shown in Table 4. The table shows that the proposed method has a higher detection precision and a stronger defect identification capability than other methods.

Table 4. The evaluation indexes of the four detection results.

Indexes	EEMD-gradient	EEMD-WEP-TEO	CEEMDAN-gradient	Proposed method
Detection deviation (mm)	21.70	19.90	9.62	9.21
PSLR (dB)	−0.0224	−0.4611	−1.0315	−6.9897
ISLR (dB)	13.3916	5.0530	10.4912	−6.1001

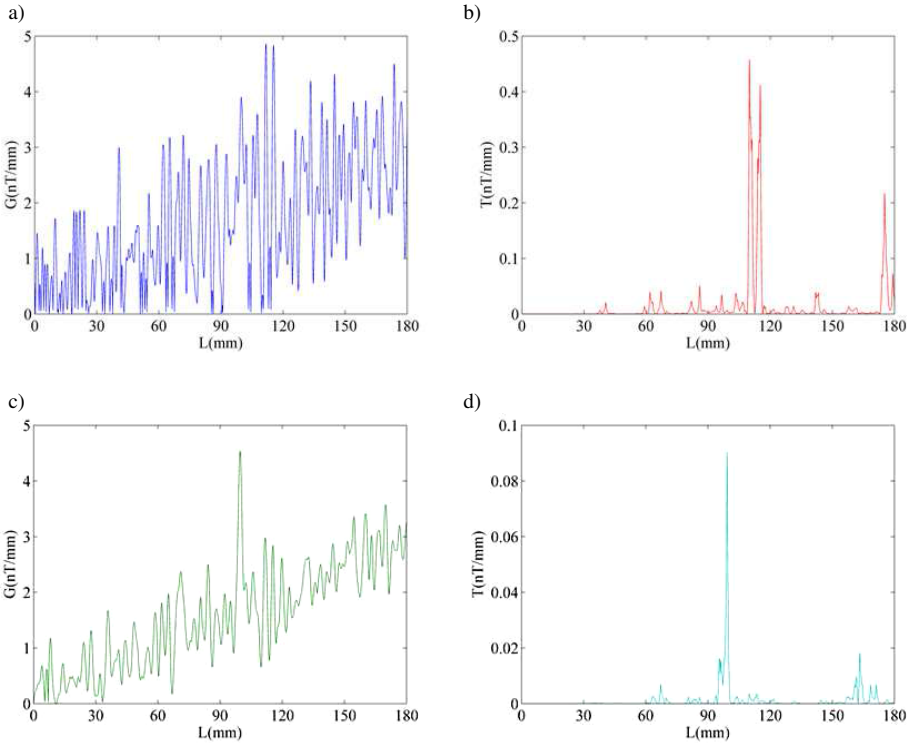

Fig. 9. The results of four detection methods in the indoor experiment: a) EEMD-gradient; b) EEMD-WEP-TEO; c) CEEMDAN-gradient; d) the proposed method.

6.2. Field testing

In order to certify the engineering practicability of the proposed method, the field testing is presented. The measurement system is shown in Fig. 10a, which contains 5 high-precision magnetic sensors TMR2309 (the measurement range is ±10 Oe and the sensitivity is 100 mV/V/Oe), an ADLINK USB-1901 data acquisition card (the resolution is 16 bits and the sampling rate is 250 kS/s), an industrial personal computer and a GPS. The pipeline segment is made of Q235 steel with a diameter of 323 mm, a wall thickness of 5 mm, buried at a depth of 1 m and operating

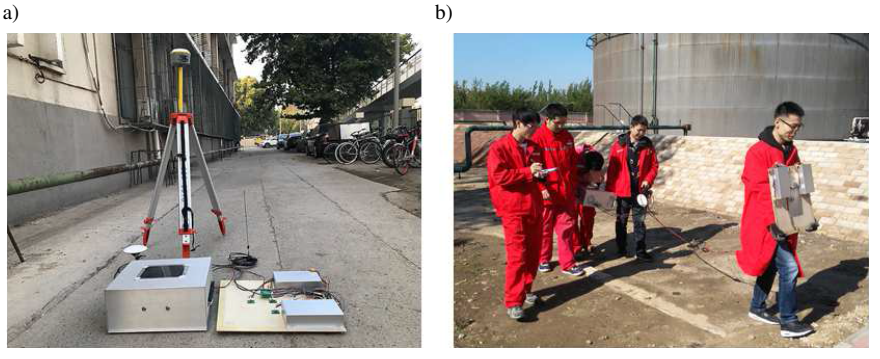

Fig. 10. The field testing of the buried pipeline: a) the measurement system; b) the field testing process.

at a pressure of 2.5 Mpa. It has been installed in Hebei Province, China. The field testing process for the buried pipeline is shown in Fig. 10b.

Figure 11 shows the magnetic signal measured by the middle sensor and the gradient signal. Since the original signal contains a great deal of random noise, it is difficult to identify the pipeline defect form Fig. 11b directly. Therefore, we carried out EEMD de-noising and CEEMDAN de-noising to filter out noise – the results are shown in Fig. 12. It can be seen that the CEEMDAN de-noised signal is smoother than that of EEMD de-noised signal. Fig. 13 shows the scaling exponents of filtered signals based on EEMD de-noising and CEEMDAN de-noising. The scaling exponent of the CEEMDAN de-noised signal is higher than that of EEMD de-noised signal, which means that the noise is reduced to a much greater extent.

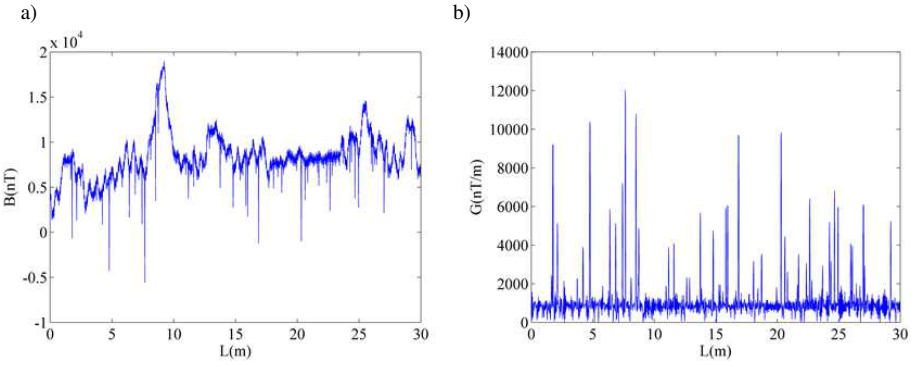

Fig. 11. The measured signal: a) the original signal; b) the gradient signal.

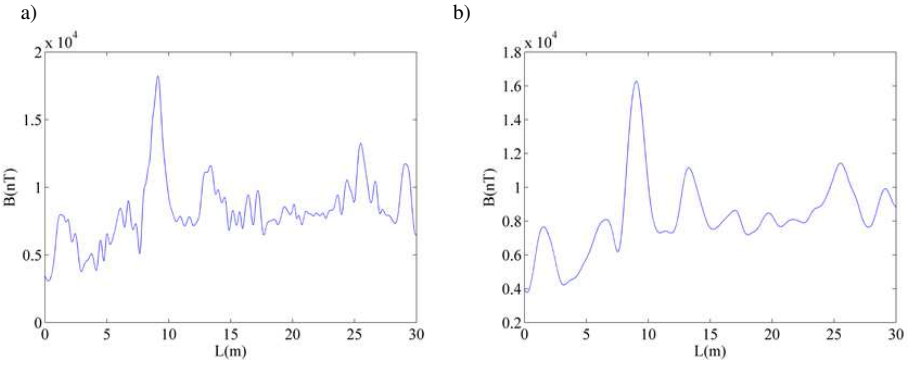

Fig. 12. The filtered signals of two de-noising methods: a) EEMD de-noising; b) CEEMDAN de-noising.

In order to clearly verify the feasibility of the proposed method, same as in the simulation and the indoor experiment, EEMD-gradient, EEMD-WEP-TEO, CEEMDAN-gradient and the proposed method were used to process the measured signal; their detection results are presented in Fig. 14. The proposed method has more evident detection results than other methods.

The detection deviation, PSLR, and ISLR for four detection results are calculated; the results are shown in Table 5. After opening the pavement, a mechanical defect was found in the pipeline at 9.2 m. The mechanical damage was a scratch that is 24 mm long, 4 mm wide, with a 1.2 mm depth. For detection deviation, the location result of the proposed method is more accurate

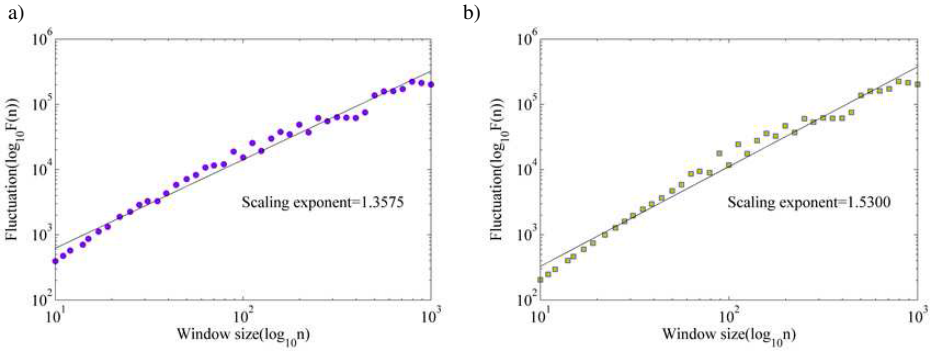

Fig. 13. The scaling exponents of filtered signals based on two de-noising methods: a) EEMD de-noising; b) CEEMDAN de-noising.

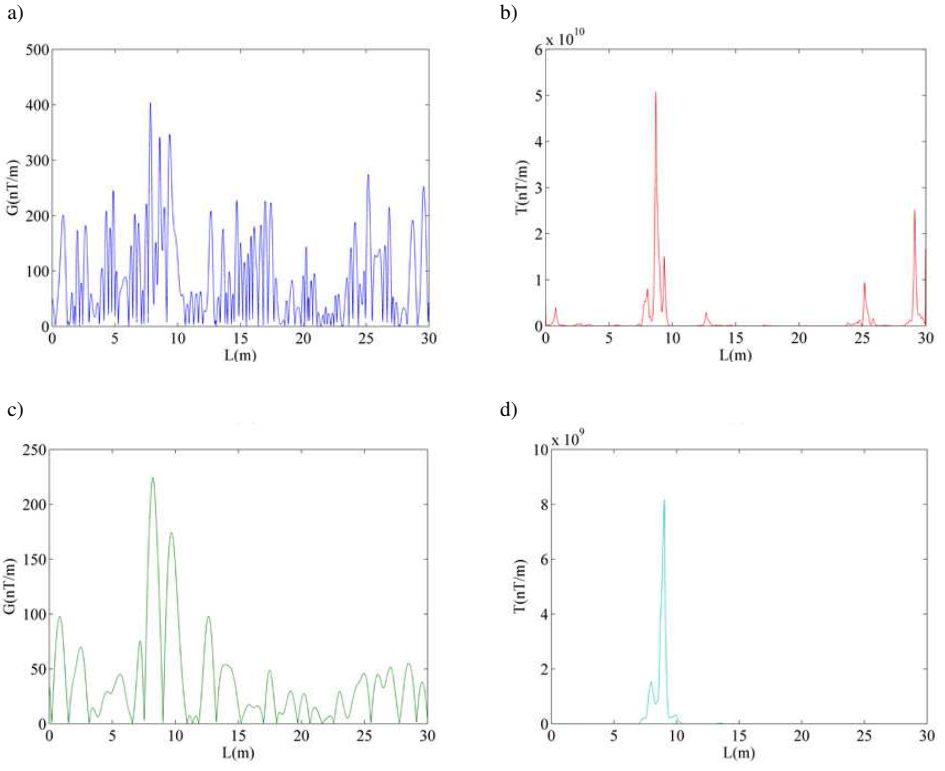

Fig. 14. The detection results of different methods: a) EEMD-gradient; b) EEMD-WEP-TEO; c) CEEMDAN-gradient; d) the proposed method.

than those of other methods. Furthermore, the PSLR of detection result based on the proposed method is higher than that of EEMD-gradient by approximately 6.6 dB, EEMD-WEP-TEO by approximately 4.2 dB, CEEMDAN-gradient by approximately 6.2 dB. The ISLR of detection result based on the proposed method is higher than that of EEMD-gradient by approximately 21.5 dB, EEMD-WEP-TEO by approximately 7.9 dB, CEEMDAN-gradient by approximately

13.8 dB. Thus, it can be seen that the proposed method can detect a defect in a buried pipeline successfully and efficiently.

Table 5. The evaluation indexes of the detection results using different methods.

Indexes	EEMD-gradient	EEMD-WEP-TEO	CEEMDAN-gradient	Proposed method
Detection deviation (m)	1.4	0.5	1	0.2
PSLR(dB)	−0.6731	−3.0446	−1.0970	−7.2771
ISLR(dB)	9.9004	−3.6931	2.2121	−11.6279

7. Conclusion

In this paper, a geomagnetic detection methodology based on CEEMDAN and WEP-TEO is presented. This method first decomposes measured signal by CEEMDAN and then selects signal IMFs by the Hurst exponent to reconstruct the filtered signal. The scale signals are obtained by gradient calculation and DWT and then fused by WEP-TEO to perform the defect detection. The CEEMDAN and Hurst exponent can reduce redundant noise and extract useful defect information. The WEP-TEO can enlarge the defect signal amplitude and improve the geomagnetic detection efficiency. The simulation experiment based on the magnetic dipole theory in the presence of background noise, the indoor experiment and the field testing were used to verify the performance of the proposed method. The results show that the proposed method exhibits an obvious superiority over other detection approaches (EEMD-gradient, EEMD-WEP-TEO, and CEEMDAN-gradient) in terms of detection deviation, PSLR, and ISLR.

Acknowledgements

This work was supported by the National Key Research and Development Program of China (2017YFC 0805005-1), Science and Technology Program of Beijing Municipal Education Commission (KZ2018 10005009), Collaborative Innovation Project of Chaoyang District Beijing China (CYXC1709), China Postdoctoral Science Foundation (2018T110018), and "Rixin Scientist" of Beijing University of Technology.

References

[1] Afzal, M., Udpa, S. (2002). Advanced signal processing of magnetic flux leakage data obtained from seamless gas pipeline. *NDT&E Int.*, 35(7), 449–457.

[2] Kim, D., Udpa, L. (2004). Remote field eddy current testing for detection of stress corrosion cracks in gas transmission pipelines. *Mater. Lett.*, 58(15), 2102–2104.

[3] Wei, L., Que, P.W., Zhang, Q., Yang, G. (2006). Ultrasonic defect detection of a petroleum pipeline in a viscoelastic medium. *Russ. J. Nondestr. Test.*, 42(10), 692–699.

[4] Murav'eva, O.V., Len'kov, S.V., Murashov, S.A. (2016). Torsional waves excited by electromagnetic-acoustic transducers during guided-wave acoustic inspection of pipelines. *Acoust. Phys.*, 62(1), 117–124.

[5] Hu, B., Yu, R.Q., Liu, J. (2016). Experimental study on the corrosion testing of a buried metal pipeline by transient electromagnetic method. *Anti-Corros. Methods Mater.*, 63(4), 262–268.

[6] Krivoi, G.S. (2008). NoPig: An above-ground inspection technique for non-piggable pipelines. *Oil. Gas-eur. Mag.*, 34(3), 122–124.

[7] Liao, K.X., Zhang, C. (2011). Standard and application by using non-contact magnetic tomography method for pipeline technical conditions diagnosis. *Proc. International Conference on Pipelines and Trenchless Technology*, China, 1049–1058.

[8] Liao, K.X., Yao, Q.K., Zhang, C. (2011). Principle and technical characteristics of non-contact magnetic tomography method inspection for oil and gas pipeline. *Proc. International Conference on Pipelines and Trenchless Technology*, China, 1039–1048.

[9] Phoong, S.M., Kim, C.W., Vaidyanathan, P.P., Ansari, R. (1995). A new class of two-channel biorthogonal filter banks and wavelet bases. *IEEE. T. Signal. Proces.*, 43(3), 649–665.

[10] Huang, N.E., Shen, Z., Long, S.R., Wu, M.C., Shih, H.H. (1998). The empirical mode decomposition and the Hilbert spectrum for nonlinear and non-stationary time series analysis. *Proc. Roy. Soc. A math. Phys. Eng.*, 454(1971), 903–995.

[11] Yang, G., Liu, Y., Wang, Y., Zhu, Z. (2015). EMD interval thresholding denoising based on similarity measure to select relevant modes. *Signal. Process*., 109(C), 95–109.

[12] Kizilkaya, A., Ukte, A., Elbi, M.D. (2015). Statistical multirate high-resolution signal reconstruction using the EMD-IT based denoising approach. *Radioengineering*, 24(1), 226–232.

[13] Humeau-Heurtier, A., Abraham, P., Mahé, G. (2015). Analysis of laser speckle contrast images variability using a novel empirical mode decomposition: Comparison of results with laser doppler flowmetry signals variability. *IEEE. T. Med. Imaging*., 34(2), 618–627.

[14] Wu, Z., Huang, N.E. (2009). Ensemble empirical mode decomposition: A noise-assisted data analysis method. *Adv. Adapt. Data Anal*., 1(1), 1–41.

[15] Chang, K.M., Liu, S.H. (2015). Gaussian noise filtering from ECG by wiener filter and ensemble empirical mode decomposition. *J. Sign. Process. Syst.*, 64(2), 249–264.

[16] Han, J., Mirko, V.D.B. Microseismic and seismic denoising via ensemble empirical mode decomposition and adaptive thresholding. *Geophysics*., 80(6), KS69–KS80.

[17] Yeh, J.R., Shieh, J.S., Huang, N.E. (2010). Complementary ensemble empirical mode decomposition: a novel noise enhanced data analysis method. *Adv. Adapt. Data Anal.*, 2(2), 135–156.

[18] Kuai, M., Cheng, G., Pang, Y.S., Li, Y. (2018). Research of planetary gear fault diagnosis based on permutation entropy of CEEMDAN and ANFIS. *Sensors*, 18(3), 782.

[19] Dai, S., Niu, D., Li, Y. (2018). Daily peak load forecasting based on complete ensemble empirical mode decomposition with adaptive noise and support vector machine optimized by modified grey wolf optimization algorithm. *Energies*, 2018, 11(1), 163.

[20] Xu, Y., Luo, M.Z., Li, T., Song, G.B. (2017). ECG signal de-noising and baseline wander correction based on CEEMDAN and wavelet threshold. *Sensors*, 17 (12), 2754.

[21] Li, Z.C., Jarvis, R., Nagy, P.B., Dixon, S., Cawley, P. (2017). Experimental and simulation methods to study the Magnetic Tomography Method (MTM) for pipe defect detection. *NDT&E Int.*, 92, 59–66.

[22] Lay-Ekuakille, A., Vendramin, G., Trotta, A. (2009). Spectral analysis of leak detection in a zigzag pipeline: A filter diagonalization method-based algorithm application. *Measurement*, 42(3), 358–367.

[23] Lay-Ekuakille, A., Griffo, G., Visconti, P. (2017). Leak detection in waterworks: comparison between STFT and FFT with an overcoming of limitations. *Metrol. Meas. Syst.*, 24(4), 631–644.

[24] Song, Q., Ding, W.X., Peng, H., Gu, J., Shuai, J. (2017). Pipe defect detection with remote magnetic inspection and wavelet analysis. *Wireless. Pers. Commun.*, 95(3), 2299–2313.

[25] Dubov, A.A., Dubov, A.A., Kolokolnikov, S.M. (2017). Non-contact magnetometric diagnostics of potentially hazardous sections of buried and insulated pipelines susceptible to failure. *Weld. World*, 61(1), 107–115.

[26] Lefebvre, D., Arsenault, H.H., Garcia-Martinez, P., Ferreira, C. (2002). Recognition of unsegmented targets invariant under transformations of intensity. *Appl. Opt.*, 41(29), 6135–6142.

[27] Yigit, E., Demirci, S., Ozdemir, C., M Tekbas. (2013). Short-range ground-based synthetic aperture radar imaging: performance comparison between frequency-wavenumber migration and back-projection algorithms. *J. Appl. Remote. Sems.*, 7(1), 073483.

[28] Zhan, L. W., Li, C. W. (2016). A comparative study of empirical mode decomposition-based filtering for impact signal. *Entropy*, 19(1), 13.

[29] Ma, W.P., Yin, S.X., Jiang, C.L., Zhang, Y.S. (2017). Variational mode decomposition denoising combined with the Hausdorff distance. *Rev. Sci. Instrum.*, 88(3), 035109.